Chinese Journal of
POLYMER SCIENCE

RESEARCH ARTICLE

https://doi.org/10.1007/s10118-024-3170-0
Chinese J. Polym. Sci. **2024**, *42*, 2021–2029

Evolution of Polymer Melt Conformation and Entanglement under High-Rate Elongational Flow

Jia-Peng Zhang[a,b,†], Li-Cheng Ma[a,b,†], Yong-Jin Ruan[a*], Yu-Yuan Lu[a,b*], and Li-Jia An[a,b*]

[a] *State Key Laboratory of Polymer Physics and Chemistry, Changchun Institute of Applied Chemistry, Chinese Academy of Sciences, Changchun 130022, China*
[b] *School of Applied Chemistry and Engineering, University of Science and Technology of China, Hefei 230026, China*

Abstract Using molecular dynamics (MD) simulations, this study explores the fluid properties of three polymer melts with the same number of entanglements, Z, achieved by adjusting the entanglement length N_e, while investigating the evolution of polymer melt conformation and entanglement under high-rate elongational flow. The identification of a master curve indicates consistent normalized linear viscoelastic behavior. Surprising findings regarding the steady-state viscosity at various elongational rates (Wi_R>4.7) for polymer melts with the same Z have been uncovered, challenging existing tube models. Nevertheless, the study demonstrates the potential for normalizing the steady-state elongational viscosity at high rates (Wi_R>4.7) by scaling with the square of the chain contour length. Additionally, the observed independence of viscosity on the elongational rate at high rates suggests that higher rates lead to a more significant alignment of polymer chains, a decrease in entanglement, and a stretching in contour length of polymer chains. Molecular-level tracking of tagged chains further supports the assumption of no entanglement under rapid elongation, emphasizing the need for further research on disentanglement in polymer melts subjected to high-rate elongational flow. These results carry significant implications for understanding and predicting the behavior of polymer melts under high-rate elongational flow conditions.

Keywords Polymer rheology; High-rate elongational flow; Entangled polymer melts; Molecular dynamics simulations; Disentanglement

Citation: Zhang, J. P.; Ma, L. C.; Ruan, Y. J.; Lu, Y. Y.; An, L. J. Evolution of polymer melt conformation and entanglement under high-rate elongational flow. *Chinese J. Polym. Sci.* **2024**, *42*, 2021–2029.

INTRODUCTION

The behavior of polymer fluids (melts or concentrated solutions) under high-rate elongational flow conditions has long been a focal point in the field of polymer rheology. One of the most remarkable challenges in polymer rheology is the entanglement effect, arising from the inability of long polymer chains to cross each other. This entanglement effect gives rise to unique dynamics and rheological phenomena, directly impacting the properties and processing of polymer materials.[1–5] At the microscale, the most successful model for describing this effect is the well-known tube model.[6,7] This model introduces three characteristic parameters to describe the properties of polymer fluids: the relaxation time of the tube segment (τ_e), the entanglement number per chain (Z), and the plateau modulus (G_e). While subsequent modifications of the tube model have introduced additional relaxation mechanisms, such as contour length fluctuations,[8] constraint release (CR),[9] convective constraint release (CCR),[10] and chain stretching,[11] these effects do not alter the fundamental nature of the entanglement effect predicted by the original tube model. Consequently, entangled polymer fluids will exhibit similar normalized linear and nonlinear rheological behaviors if they possess the same Z. However, recent experiments[12,13] on melts and solutions with the same Z have revealed drastically different steady-state elongational viscosity. Specifically, for highly concentrated solutions or melts, the systems exhibit an extensional rate thinning effect, whereas for relatively dilute solution systems, they display an extensional rate thickening effect. This contradiction poses a significant challenge to the theoretical framework of the tube model.[14–16] The success of the tube model in addressing rapid elongational flow is thus called into question, as it fails to fully account for the observed discrepancies in the behavior of polymer melts and solutions under high-rate elongational flow conditions.

In the context of high-rate elongational flow, the mechanisms underlying the occurrence of the extensional rate thinning/thickening effects in entangled polymer fluids have been the subject of extensive investigation. One commonly proposed explanation revolves around the concept of finite extensibility of polymer chains.[17] Specifically, it has been suggested that solutions with higher concentrations exhibit a smaller entanglement length N_e, which in turn leads to a reduced maximum chain stretch ratio, thereby limiting the extensibility of the chains.[17] However, the finite extensibility ar-

* Corresponding authors, E-mail: yjruan@ciac.ac.cn (Y.J.R.)
E-mail: yylu@ciac.ac.cn (Y.Y.L.)
E-mail: ljan@ciac.ac.cn (L.J.A.)
† These authors contributed equally to this work.
Received April 28, 2024; Accepted May 21, 2024; Published online August 20, 2024

gument has been challenged by the findings of Ianniruberto *et al.*,[16,18,19] who proposed an alternative mechanism involving flow-induced friction reduction. According to this perspective, the alignment of Kuhn segments in a strong flow results in a decrease of the segmental friction coefficient, thereby influencing the overall behavior of the polymer fluids under high-rate elongational flow conditions. This viewpoint, however, has been met with skepticism by proponents of alternative models such as the slip-link model,[20] the extended interchain pressure (EIP) model,[21] and the work of Shahid *et al.*,[22] all of which argue against the notion of friction reduction. The debate is further complicated by the utilization of molecular dynamics (MD) simulation results, with Ianniruberto *et al*.[18] drawing support from the work of O'Connor *et al.*,[23] while O'Connor *et al*.[24] themselves argued that there is no substantial evidence of a significant change in monomeric friction or large reductions in entanglement density.

Moreover, O'Connor *et al*.[23,24] put forth the proposition that under high-rate elongational flow, chains may become fully extended, leading to a viscosity that scales with the square of the chain length. This perspective suggests a greater decrease in viscosity with rates for longer and stiffer chains, thereby introducing additional complexity to the understanding of polymer melt behavior under high-rate elongational flow conditions. Additionally, the contributions of factors such as time-temperature superposition breakdown[25] and interchain forces have been highlighted by Wang *et al*.[26] as important considerations in the context of elongational stress. In addition to the aforementioned debates surrounding the mechanisms of extensional rate thinning and thickening, the question of whether entangled polymer melts or concentrated solutions can attain a steady-state elongational state, or if the ultimate fate of these systems involves phenomena such as fracture or necking, remains a longstanding unresolved challenge within the field of nonlinear rheology. This unresolved issue underscores the complexity and richness of the behavior of entangled polymer fluids under high-rate elongational flow, and highlights the need for further research and theoretical development in this area.

MD simulation offers the advantage of directly tracing the microstructural conformation and evolution of polymer chains during the stretching process. However, it does not provide direct information on the entanglement evolution. In a different but related study, Baig *et al*.[27] demonstrated that the *Z* exhibits shear-thinning behavior similar to shear viscosity, with the entanglement number determined by the Z1 code.[28] Notably, there is a lack of similar analysis in elongational simulations[23,26] due to the complex triclinic periodic boundary conditions in the general Kraynik-Reinelt (GKR) boundary condition.[29,30] Recently, Wang *et al*.[26] focused on the entanglement lockup before the stretching ratio λ=18.8 (not reaching steady-state). Through the combination of bonded force and characterization of chain conformation, they observed that chain tension can build up due to the unique hairpin structure of each load-bearing chain.[26] However, due to the absence of a convenient method, they were unable to delve into the complicated clusters of multichain interactions during the earlier stages of elongation. Therefore, there is a need for direct information about entanglement evolution and the interaction between chains under elongational flow. Understanding when and how chain disentanglement occurs will provide valuable insights into elongational research.

To address this gap, we recently present an analysis of primitive paths (PPs) by combining energy minimization with the Frenet trihedron geometric analysis (FT-PPA).[31] This method outputs the index of each pair of entangling kinks and the number of multiple mutual entanglements (MuEs) between two tagged chains in entangled polymer melts under equilibrium and shear conditions. Furthermore, we discovered that the distribution of MuEs is closely related to the appearance of shear bands. Therefore, FT-PPA can theoretically describe the entanglement evolution in stretched polymer fluids, thus aiding in resolving the issues addressed in this study.

In this study, we aim to investigate the conformation and entanglement evolution of polymer melts under high-rate elongational flow, with a focus on the key factors influencing the behavior of entangled polymer melts under rapid elongational conditions. To achieve this, we employ MD simulations to explore the properties of three polymer melts with the same number of entanglements, *Z*, by adjusting the entanglement length N_e. To begin, we validate that the three melts exhibit the same normalized linear rheological properties. Subsequently, we utilize the GKR boundary condition to avoid significant size effects during the elongational simulation, as well as to mitigate the occurrence of fracture or necking phenomena commonly observed in experimental setups. Our focus is on the elongational stress growth coefficient, steady stress, and normalized elongational behavior of these three melts. Our results demonstrate that, despite having the same *Z*, their nonlinear rheological properties differ significantly from classical theoretical predictions, but are consistent with rheological elongational experiments. Finally, to explore the rheological properties of entangled polymer melts under rapid elongational flow, we quantitatively analyze the chain orientation, the entanglement number per chain using our FT-PPA,[31] and the contour length of polymer chains. The results reveal that under these conditions, polymer chains undergo nearly complete disentanglement and are fully stretched, leading to a steady-state elongational viscosity that is almost independent of the elongational rate, but can be normalized by scaling with the square of the chain contour length. These phenomena are often accompanied by fracture or necking in real experimental processes. Consequently, it is reasonable to infer that entangled polymer melts cannot enter a steady-state elongational stage under rapid stretching conditions, as the system is highly unstable within this regime. These findings have significant implications for the design and processing of polymer materials under extreme flow conditions.

SIMULATION MODEL AND METHOD

We employ the Kremer-Grest (KG) model[32] to simulate entangled polymer melts at a monomer density of $0.85d^{-3}$. All monomer pairs interact through a truncated and shifted pairwise Lennard-Jones (LJ) potential with a cutoff distance r_c =

https://doi.org/10.1007/s10118-024-3170-0

$2^{1/6}d$, as described by the following equation:

$$U_{LJ}(r) = 4u\left[\left(\frac{d}{r}\right)^{12} - \left(\frac{d}{r}\right)^{6}\right],\ r \leqslant r_c = 2^{1/6}d \quad (1)$$

where u represents the energy scale and d denotes the length scale. To model chain connectivity, we utilize the finitely extensible nonlinear elastic (FENE) potential, which is expressed as:

$$U_{FENE}(r) = -0.5kr_0^2\ln\left[1 - (r/r_0)^2\right] \quad (2)$$

In this equation, the spring constant is denoted by $k = 30u/d^2$, and the fully stretched bond length is $r_0 = 1.5d$. To adjust the entanglement length N_e, a bending potential is incorporated,[33] given by:

$$U_{bend}(r) = k_b(1 - \cos\theta) \quad (3)$$

where θ represents the angle between two subsequent bonds. The Kuhn length of polymer chains increases with the strengthening of the bending potential k_b. In other words, under the same chain length conditions, a higher k_b value results in larger root-mean-square radius of gyration R_{g0} and occupied volume of the polymer chains. Consequently, with an increased probability of polymer chains encountering each other, the number of chain entanglement also rises. Thus, a larger k_b will lead to a smaller N_e. Previous work by Everaers *et al.*[34,35] demonstrated that for k_b=1.5, 0.75 and 0.0, the entanglement lengths N_e=28, 45 and 63, respectively. Consequently, we set the chain length N=180, 300 and 500 for k_b=1.5, 0.75 and 0.0, respectively. For the sake of brevity, we will not emphasize the bending stiffness k_b further, as each k_b value corresponds to a specific chain length N. The characteristic properties of the three melts are summarized in Table 1. Due to different k_b values, the three melts have varied Kuhn lengths, leading to the deviation of their root-mean-square radius of gyration R_{g0} from the $N^{0.5}$ scaling.

Length, energy, and time are normalized using the monomer diameter (d), energy parameter (u), and the LJ timescale [$\tau = (md^2/u)^{0.5}$], respectively. The monomer mass m is set to 1. The temperature is selected such that $k_BT/u = 1$ and is regulated by the Nosé-Hoover thermostat.[36–37] Initial configurations are generated by randomly assigning positions and further equilibrated using the double-bridging-MD hybrid algorithm.[33] This algorithm is applied to the sample obtained above at three stages, each lasting Rouse time τ_R, with the spring constant k increasing from 10 to 20 to 30. Subsequently, further equilibration is conducted for τ_R. The chains exhibit the same mean square internal distance as in previous work.[33] The entanglement number per chain Z is measured using energy minimization,[34–35] and geometry minimization (Z1+ code[38]). The results in Table 1 confirm that the three melts have the same Z per chain.

Table 1 Simulation parameters used in this work: chain length N, bending stiffness k_b, root-mean-square radius of gyration R_{g0}, initial box length L_0, entanglement number per chain using energy minimization (Z_{PPA}), geometry minimization (Z_k), and our FT-PPA (Z_{F0})[34]. The subscript 0, PPA, k, and F represent equilibrium, primitive path analysis, kink, and Frenet, respectively.

N	k_b	R_{g0} (d)	L_0 (d)	Z_{PPA}	Z_k	Z_{F0}
180	1.50	8.82	53.28	6.56	12.58	10.16
300	0.75	10.22	59.40	6.65	12.47	11.32
500	0.00	11.88	71.48	6.66	12.39	12.01

For the elongational flow simulations, we utilize the UEF (under extensional flow) package[39] of LAMMPS (large-scale atomic/molecular massively parallel simulator), where the particles move according to the SLLOD equation[40] with the GKR boundary condition.[29,30] The initial simulation box is cubic with an initial length L_0; the box basis vectors are deformed with an elongational velocity gradient tensor, and the deformed basis vectors are transformed back into the initial cubic box when they correspond to the reproducible lattice. The melts are stretched at a constant Hencky rate $\dot{\varepsilon} = d\varepsilon/dt = d\ln(L/L_0)/dt$ along the z-direction, and the perpendicular directions (x and y) are both contracted by $\dot{\varepsilon}^{-0.5}$ to preserve volume, where Hencky strain $\varepsilon = \ln(L/L_0)$ and L is the box length at time t. All simulations are performed using the LAMMPS[41–42] (*fix nvt/uef* command) with 4 independent samples, and the integration time step (Δt) is set to 0.005.

RESULTS AND DISCUSSION

Linear Viscoelasticity

The characteristic parameters of entangled polymer melts must be determined prior to conducting elongational simulations. In MD simulations, the entanglement time scale τ_e is often derived from the scaling crossover[7] in the mean square displacement versus time plot. However, this crossover is highly ambiguous. For the KG model, different researchers have obtained varying values for τ_e. For example, Hsu and Kremer[43] reported τ_e=1980 with a bending strength k_b=1.5, while Ge *et al.*[44] obtained τ_e=6000 and 4000 with k_b=0.75 and 1.5, respectively. The discrepancies are evident in the work of O'Connor *et al.*,[24] who assumed τ_e=6000 with k_b=0.75 and τ_e=1980 with k_b=1.50 in their elongational simulation. Furthermore, their data[24] do not align with the linear viscoelastic (LVE) line, which is a crucial reference for nonlinear data. Consequently, it is not currently feasible to accurately determine the characteristic parameters of entangled polymer systems using the scaling crossover. These parameters are critical for understanding the underlying mechanisms governing the viscoelastic properties of polymer melts.

To quantitatively compare with experimental results, it is necessary to conduct small-amplitude oscillatory shear simulations to obtain the equilibrium properties of entangled polymer melts, including the storage modulus $G'(\omega)$ and the loss modulus $G''(\omega)$. These moduli can be fitted using the Likhtman-McLeish (LM) theory or the Baumgaertel-Schausberger-Winter (BSW) equation. This approach is essential for obtaining reliable data that can be compared with experimental observations.

However, the process of conducting oscillatory shear simulations is time-consuming. Furthermore, the linear modulus $G(t)$ can be expressed by the correlation function of the stress $\sigma_{xy}(t)$ in equilibrium, *i.e.*, $G(t) = \langle\sigma_{xy}(t)\sigma_{xy}(0)\rangle$. Therefore, we can directly calculate $G(t)$ by computing the correlation functions. A requirements method[45,46] is utilized to calculate the correlation functions, and the resulting data is presented in Fig. 1(a). For $t < \tau_e$, $G(t)$ exhibits a behavior of $t^{-0.5}$, as described by the Rouse model, which characterizes the chain dynamics. For $\tau_e < t < \tau_{d0}$, the chains move in a tube regime, and $G(t)$ should ideally display a plateau value. However, due to the finite chain length, a clearly defined plateau value is not evident in our data.

https://doi.org/10.1007/s10118-024-3170-0

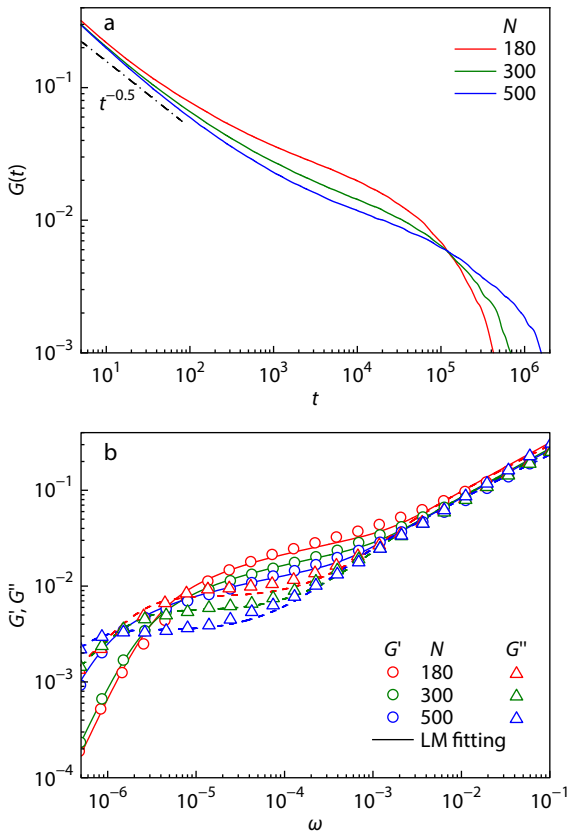

Fig. 1 (a) The linear moduli $G(t)$ obtained from the simulation and (b) the storage moduli $G'(\omega)$ (solid line) and the loss moduli $G''(\omega)$ (dash line) for N=180, 300, and 500. The lines represent fits of the Likhtman-McLeish (LM) model. The open points correspond to the Maxwell mode results.

Subsequently, we fit $G(t)$ with the sum of Maxwell modes ($G(t) = \Sigma G_i \exp(-t/\tau_i)$), as depicted in Fig. 1(b). $G'(\omega)$ and $G''(\omega)$ can be calculated accordingly by

$$G'(\omega) = \sum_{i=1}^{10} G_i \frac{(\omega\tau_i)^2}{1+(\omega\tau_i)^2} \quad (4)$$

$$G''(\omega) = \sum_{i=1}^{10} G_i \frac{\omega\tau_i}{1+(\omega\tau_i)^2} \quad (5)$$

We then analyze these LVE data using the LM theory.[7] The adjustable parameters G_e, Z, and τ_e are provided in Table 2. The Rouse time τ_R and the disengaged time τ_{d0} at equilibrium can be calculated based on Z and τ_e. Table 2 will serve as a reference for the KG model, as G_e and τ_e should be consistent for given melts with varied chain lengths. In this analysis, we use 10 modes because the data span 5 orders of magnitude.

Table 2 Characteristic parameters obtained from the LM theory: the entanglement number per chain Z_{LM}, plateau modulus G_e, relaxation time of a tube segment τ_e, Rouse time $\tau_R = \tau_e Z_{LM}^2$, and disengaged time $\tau_{d0} = 3Z_{LM}\tau_R(1-3.38/Z_{LM}^{0.5}+4.17/Z_{LM}-1.55/Z_{LM}^{1.55})$.

N	Z_{LM}	G_e ($md^{-1}\tau^{-2}$)	τ_e (τ)	τ_R (τ)	τ_{d0} (τ)
180	7.8	0.0428	870	5.30×10^4	3.13×10^5
300	7.6	0.0308	1270	7.45×10^4	4.27×10^5
500	8.2	0.0195	2970	1.99×10^5	1.28×10^6

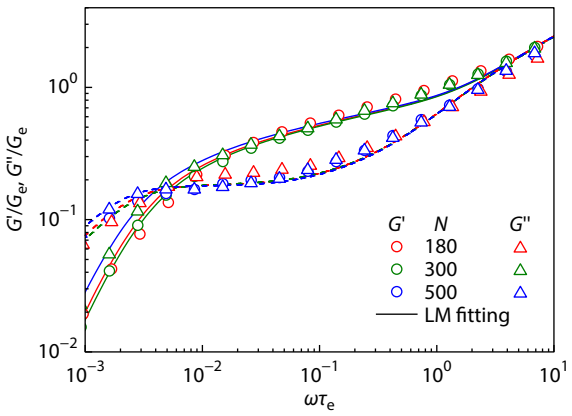

Fig. 2 The normalized storage modulus G'/G_e and loss modulus G''/G_e as a function of the normalized frequency $\omega\tau_e$ for N=180, 300, and 500. The lines represent the results of the LM theory.

Finally, Fig. 2 compares the $G'(\omega)$ and $G''(\omega)$ using dimensionless parameters, where the frequency is normalized by $1/\tau_e$, and the moduli are normalized by G_e. A master curve is obtained, confirming that the three melts have the same Z and the same normalized linear rheological properties.

Startup and Steady-State Elongational Flow

In this section, we first define the Rouse–Weissenberg number as $Wi_R = \dot{\varepsilon}\tau_R$. Fig. 3 illustrates the elongational stress growth coefficient $\eta_{ex} = \sigma_{ex}/\dot{\varepsilon} = [\sigma_{zz} - 0.5(\sigma_{xx} + \sigma_{yy})]/\dot{\varepsilon}$ (the subscript ex means extension), which is represented as a function of time across a range of Wi_R values from 0.2 to 59.2. It is important to note that a critical aspect of the MD simulations is the precise control of temperature. However, due to the inherent challenges in maintaining temperature control within the system, it is anticipated that the actual temperature will exceed the designated temperature (denoted as temperature 1) when $\dot{\varepsilon}>10^{-3}$.[30] Consequently, simulations at higher Wi_R values were not conducted. The dashed lines in Fig. 3 represent predictions derived from $G(t)$ in Fig. 1, specifically $\eta_{LVE}(t) = 3\int G(t)dt$. Notably, the data corresponding to the lowest strain rates closely align with the

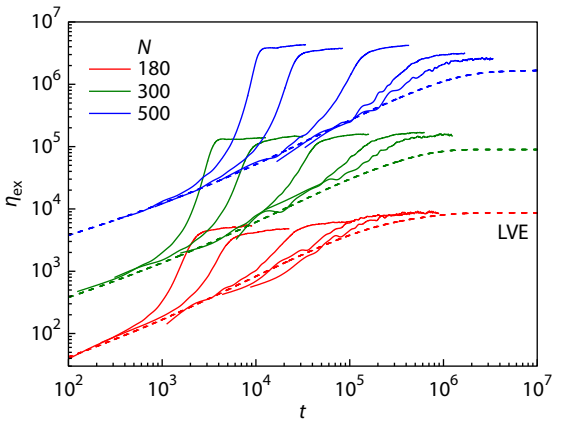

Fig. 3 Elongational stress growth coefficient as a function of time. The Wi_R for N=180, 300, and 500 (from right to left) are 0.6, 1.2, 4.7, 23.7, and 59.2. The dashed lines represent the linear viscoelastic regime. For clarity, the data have been shifted up by 1 decade for N = 300 and 2 decades for N = 500, and the results of lower rates are not shown.

https://doi.org/10.1007/s10118-024-3170-0

LVE line.

Furthermore, the data corresponding to low strain (short time) demonstrate conformity with the LVE line, a phenomenon that was not addressed in Ref. [22]. As the elongational stress data gradually increases above the LVE lines due to stretch thickening, these observations confirm the linear viscoelasticity of our simulation. Additionally, it is observed that η_{ex} approaches a steady-state for each rate at Hencky strain values exceeding 4. This finding underscores the establishment of steady-state conditions within the system. These results provide valuable insights into the behavior of the polymer melts under elongational flow conditions and contribute to a comprehensive understanding of its viscoelastic properties.

The steady-state viscosity η_{ex}^{ss} (the superscript ss means steady-state) of the system was obtained as the melts reached unlimited strain under the GKR boundary condition. In this study, the value of η_{ex} at Hencky strain ε=5.5–6 was taken as the steady-state viscosity η_{ex}^{ss}. However, it was observed in the experiment[13,47] that η_{ex}^{ss} was not clearly defined even up to ε=5 at high elongational rates. The Doi-Edwards (DE) theory[1] predicts three distinct regions for the steady-state viscosity η_{ex}^{ss} versus Hencky rate $\dot{\varepsilon}$: (I) When $\dot{\varepsilon} < \tau_{d0}^{-1}$, η_{ex}^{ss} is equal to 3 times the zero-shear viscosity η_0. (II) When $\tau_{d0}^{-1} < \dot{\varepsilon} < \tau_R^{-1}$, the tube segments are oriented to the stretching direction, resulting in a decrease in viscosity as $\dot{\varepsilon}^{-1}$. (III) With further increasing $\dot{\varepsilon} > \tau_R^{-1}$, the chains start to stretch, leading to an upturn in viscosity.

Due to limitations in computational resources, data for region I could not be obtained. However, the overlapping of normalized storage modulus and loss modulus (see Fig. 2) confirms the overlapping of normalized steady-state viscosity η_{ex}^{ss} of three melts. Surprisingly, our data (see the inset of Fig. 4) revealed different trends at higher rates. For N=180 and 300, η_{ex}^{ss} did not change with increasing strain rate at Wi_R<1, and gradually decreased to a stable value with increasing strain rate at Wi_R>1. Conversely, for N=500, η_{ex}^{ss} gradually increased to a stable value with increasing Wi_R>1. This unexpected result is particularly intriguing as the three systems possess the same number of entanglement, indicating that existing tube models are insufficient to explain these observations. Nevertheless, the results are in good agreement with existing experimental data.[13]

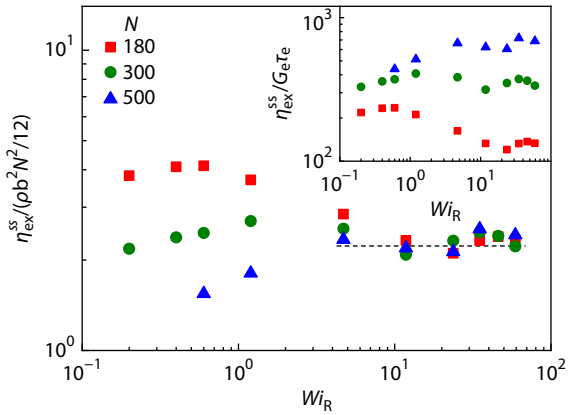

Fig. 4 Elongational steady-state viscosity η_{ex}^{ss} normalized by $\rho b^2N^2/12$ as a function of Wi_R for N=180, 300, and 500. The inset shows the normalized steady-state viscosity as a function of Wi_R. Due to limited computational resources, there is no data available at Wi_R=0.2 and 0.4 for N=500.

Furthermore, as shown in Fig. 4, at higher elongational rates, a non-normalized phenomenon was observed, which is believed to be associated with the entanglement in polymer melts. This observation is consistent with the findings of previous studies. Ianniruberto *et al.*[19] introduced the IV region, where the polymer chain is fully extended without entanglement, and the system exhibits an asymptotic viscosity, denoted as η_∞. According to the Fraenkel model, which assumes a nearly inextensible Rouse model and neglects entanglement effects, Ianniruberto and Marrucci[18] derived the expression $\eta_\infty = \zeta\rho b^2N^2/12$, where ζ is the friction coefficient and b is the averaged bond length. We set b=0.964, which represents the equilibrium value. Furthermore, we confirm that the average bond length b remains largely unaffected by the bending potential and elongational rates employed in this study. This asymptotic result was also reported by O'Connor *et al.*[23] This finding provides evidence to support the hypothesis that at higher elongational rates, the entanglement in polymer melts decreases, leading to the full extension of polymer chains. Furthermore, based on simulations[32] utilizing the Langevin thermostat, Ianniruberto and Marrucci[18] indicated that the friction coefficient ζ at equilibrium state is approximately 15, a value consistent with our unpublished data (around 13) obtained using the Nosé-Hoover thermostat. This value significantly exceeds the friction coefficient of around 2 observed for individual monomers at high elongation rates in Fig. 4, suggesting a notable reduction in monomer friction coefficient. However, elucidating the underlying reasons for the distinct elongation thinning and thickening behaviors requires further in-depth investigation.

Conformation and Entanglement Analysis

To demonstrate the evolution of polymer melt conformation by analyzing the chain orientational order, specifically the nematic order parameter (P_2, the subscript 2 means the second-order Legendre function). The nematic order parameter was calculated using the formula $P_2 = 0.5(3\cos^2\theta - 1)$, where θ represents the angle between the z-axis and the end-to-end vector of the chain. Fig. 5 illustrates the steady-state orientational order (P_2^{ss}) at various elongational rates. It is important to note that at equilibrium, P_2^{ss} is 0, indicating a completely random chain orientation. However, as the elongational rate increases, P_2^{ss} approaches unity, particularly at high Wi_R values greater than 4.7. This observation is consistent with the findings of Baig *et al.*[27] and our shear simulations (which have not been published), both of which demonstrate that P_2^{ss} approaches approximately 0.9 at high shear rates.

This comparison suggests that under stretching conditions, the chain orientation becomes more pronounced. These results also indicate a clear correlation between the elongational rate and the degree of chain orientation, with higher rates leading to a more significant alignment of the polymer chains. When Wi_R exceeds 4.7, it is highly likely that the system undergoes complete disentanglement due to the nearly fully extended polymer chains.

To substantiate our above conjecture regarding complete

https://doi.org/10.1007/s10118-024-3170-0

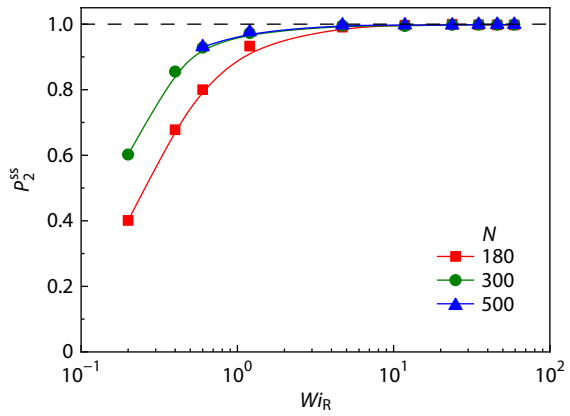

Fig. 5 Steady-state chain orientational order P_2^{ss} as a function of Wi_R for N=180, 300 and 500.

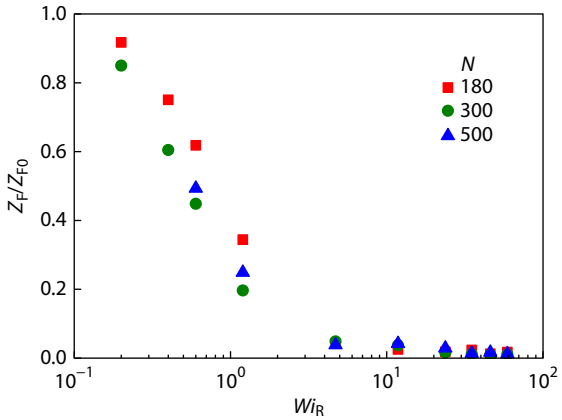

Fig. 6 Normalized steady-state number of entanglements per chain as a function of Wi_R for N=180, 300 and 500.

disentanglement, additional direct evidence is required. While the Z1/Z1+ code[28,38] is a useful tool that, in principle, can provide information on the entanglement number under the GKR boundary condition. However, existing versions of the Z1+ code are unable to handle the parallelepiped simulation box. Consequently, we have developed a new entanglement analysis method to address this limitation. Our method comprises two key steps. Firstly, we obtain the smooth primitive path (PP) for all chains in each system. Subsequently, we conduct PP analysis using the Frenet trihedron. To obtain the smooth PP, we follow the approach outlined in Ref. [33]: initially, we fix the chain ends in space; then, we eliminate the intrachain excluded volume interactions, remove the bending potential, retain the interchain excluded-volume interactions, and preserve the FENE potential. Finally, we minimize the energy of the system by cooling it towards T=0. As PPs cannot pass through each other, sharp bends naturally occur at the entanglement points where two PPs come into contact. In other words, a PP can be viewed as a sequence of straight segments connected by these sharp bends. To identify these bends, we introduced[31] the Frenet trihedron, which describes the local geometric properties of a curve in three-dimensional space.

At equilibrium, the results obtained using our FT-PPA method indicate that the entanglement number per chain is very similar for systems with different chain rigidities (N=180, 300 and 500), the values of Z_{F0} are 10.2, 11.3 and 12.0, respectively. This reaffirms that the three melts have the same entanglement number, Z. It is important to note that the differences in the values of Z in Table 1 arise from the application of different definitions of entanglement. The steady-state Z_F as a function of elongational rate is depicted in Fig. 6. It is evident that Z_F decreases significantly with the applied elongational flow, and there is no discernible entanglement at Wi_R>4.7. This finding provides further evidence in support of our earlier conjecture. The reason for this phenomenon lies in the significantly oriented chains along the uniaxial elongational flow, which can slide past each other and thus become almost disentangled compared to the equilibrium case.

These results offer valuable insights into the evolution of entanglement in polymer melt conformation under different flow conditions. The observed decrease in entanglement with increasing elongational flow has significant implications for understanding the rheological behavior of polymer materials, particularly in processes involving high rates of deformation. Furthermore, the development of our new entanglement analysis method addresses a critical limitation in existing tools, thereby enhancing the capability to study and characterize entanglement in polymer systems with complex simulation geometries.

Another crucial aspect of entangled polymer rheology is the evolution of the primitive chain contour length. We initially divide the chain into Z_{LM} blobs comprising N/Z_{LM} monomers and define the line connecting the centroids of these blobs as a proxy for the primitive chain's contour length. Fig. 7 illustrates the steady-state contour length of the primitive chain as a function of Wi_R. At low elongation rates, polymer chain stretching is negligible. However, as Wi_R>1, the primitive chain is elongated by the flow field, leading to an increase in its contour length. Notably, at sufficiently high elongation rates, under steady-state conditions, polymer chains fully orient and disentangle, resulting in no further elongation of the contour length, with the overall length remaining nearly constant with increasing shear rate. Comparing polymer chains of different lengths, we also observe that the maximum elongational ratio of polymer chains increases with increasing entanglement length, consistent with the findings in

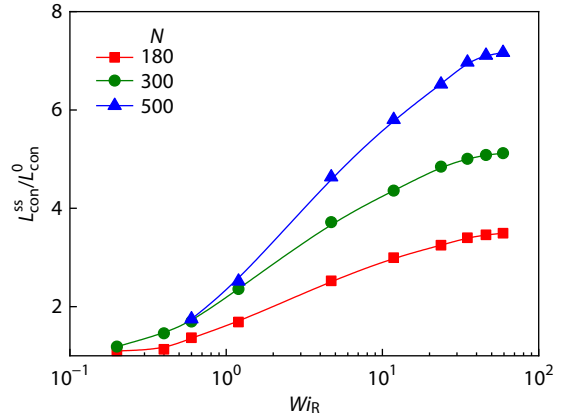

Fig. 7 Normalized steady-state contour length of the primitive chain as a function of Wi_R for N=180, 300 and 500.

https://doi.org/10.1007/s10118-024-3170-0

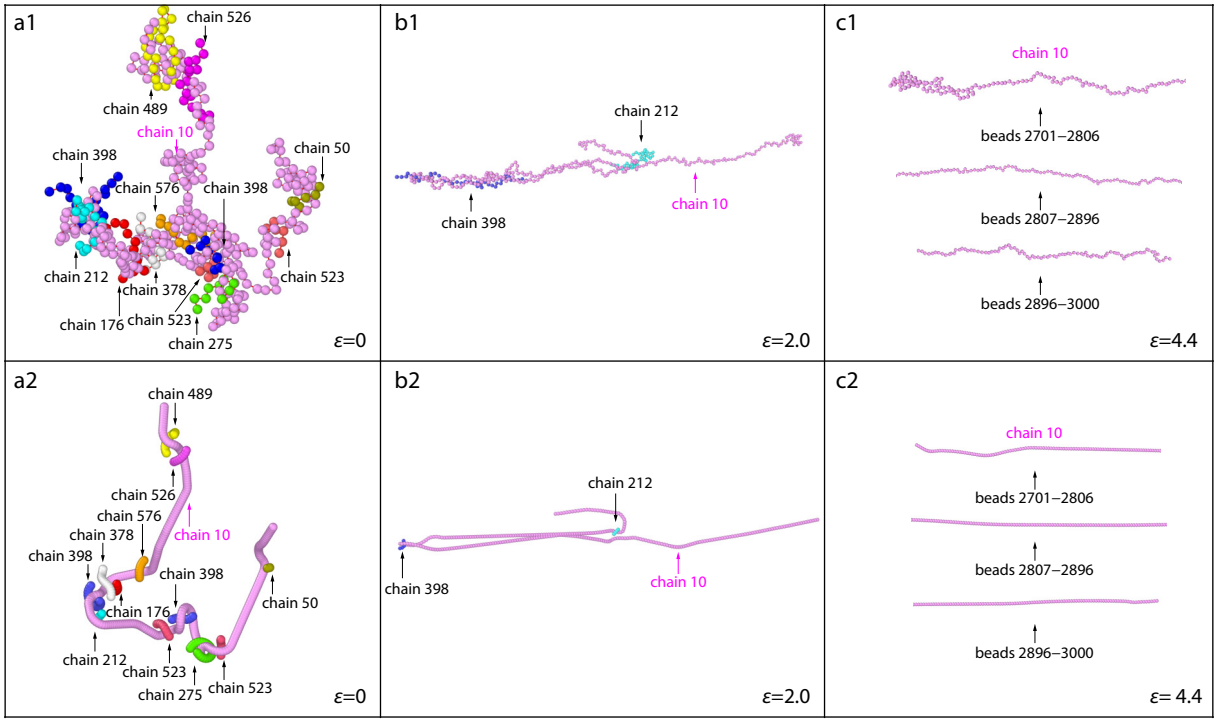

Fig. 8 Visualization of chain 10 (pink) as illustrations to reveal the nature of the interchain interactions at ε=0.0 (equilibrium), 2.0 and 4.4 with Wi_R=11.8 for N=300. (a1, b1, c1) Snapshots obtained directly from MD simulations and (a2, b2, c2) corresponding snapshots obtained using our FT-PPA method. Detailed descriptions can be found in the text.

Ref. [17]. Additionally, it is worth mentioning that the quantitative relationship between the steady-state orientation, steady-state entanglement, steady-state elongational ratio, and steady-state viscosity of polymer systems with high entanglement number during rapid elongation is highly intricate, a topic we plan to delve into further.

To provide a more detailed understanding of the disentanglement process at the molecular level, we conducted tracking of the tagged chain for N=300 at Wi_R=11.8, as illustrated in Fig. 8. Our FT-PPA method facilitates the labeling of entanglement locations, enabling direct acquisition of neighbor chain and monomer indices around the tagged chain. At equilibrium (Figs. 8a1 and 8a2), the tagged chain intertwines with other chains. Subsequently, upon application of elongational stress, the tagged chain gradually extends along the elongational direction and undergoes disentanglement. At low strain (Figs. 8b1 and 8b2), a hairpin structure forms, restricting the sliding of the target polymer chain. Furthermore, as the stretching stress reaches a steady state, as depicted in Figs. 8(c1) and 8(c2), there are almost no entangled chains around the tagged polymer chains, indicating full extension of the chain, leading to the orientation parameter $P_2^{ss} \sim 1$. This result supports the assumption of no entanglement in the work of Ianniruberto *et al.*[16] However, in real experimental processes, the system is highly unstable within this regime. Consequently, it is reasonable to infer that entangled polymer melts cannot enter a steady-state elongational stage under rapid stretching conditions. In other words, the fate of the stretched entangled polymer system often does not involve reaching a steady state, but rather terminates in the familiar fracture or necking phenomena. The relative ease with which simulations can enter a steady state is attributed to the use of the GKR boundary condition, which can avoid significant size effects during the elongational simulation, particularly mitigating the occurrence of fracture or necking phenomena commonly observed in experimental setups. Therefore, further research should focus on the disentanglement in polymer melts under high-rate elongational flow. For example, it is important to investigate whether a hairpin structure can exist stably, for how long, and to what extent it affects the macroscopic stress values of the system.

CONCLUSIONS AND OUTLOOK

This study has successfully characterized the linear viscoelasticity and elongational behaviors of polymer melts with the same entanglement number per chain Z, providing valuable insights into the evolution of polymer melt conformation and entanglement under high-rate elongational flow. The confirmation of a master curve for normalized linear viscoelasticity data indicates consistent behavior across different bending potential KG models, laying a solid foundation for future research in this area. Unexpected findings regarding the steady-state viscosity at high elongational rates challenge existing tube models and highlight the necessity for further investigation to accurately describe polymer melt behavior under such conditions. Evidence presented in this study suggests a correlation between stretching rate and chain orientation, with higher rates leading to increased chain alignment. Moreover, the decrease in entanglement observed under rapid stretching contradicts conventional understanding and emphasizes the need for additional research on disentanglement in polymer melts subjected to high-

rate elongational flow. In addition, the chain with larger entanglement length shows a larger chain stretch ratio. Overall, this research significantly advances our understanding of polymer melt rheology and sets the stage for further exploration into the evolution of entanglements in polymer systems.

Moving forward, it is imperative to delve deeper into the specific molecular mechanisms behind the behaviors observed in this study. The FT-PPA method utilized here shows promise as a powerful tool for addressing unresolved challenges in analyzing polymer melts with the same entanglement number per chain. Further research is needed to develop accurate predictive models that can effectively capture the complex interplay between polymer conformation, entanglement, and rheological properties. Investigating the impact of entanglements on polymer behavior under high-rate elongational flow will not only enhance our fundamental understanding but also pave the way for practical applications in various fields of polymer rheology. Future studies[48] should focus on elucidating the relationship between stretching rate, chain alignment, and entanglement dynamics to provide a comprehensive framework for predicting and controlling the rheological behavior of entangled polymer systems. By continuing to explore these avenues, we can unlock new insights and innovations that will advance the field of polymer melt rheology and its diverse applications.

Conflict of Interests

Li-Jia An is an editorial board member for *Chinese Journal of Polymer Science* and was not involved in the editorial review or the decision to publish this article. All authors declare that there are no competing interests.

Data Availability Statement

The data supporting the findings of this study are available from the corresponding author upon reasonable request. Please find the author's contact information: yylu@ciac.ac.cn (Y.Y.L.).

ACKNOWLEDGMENTS

This work was financially supported by the National Key R&D Program of China (Nos. 2020YFA0713601 and 2023YFA1008800), the National Natural Science Foundation of China (Nos. 22341304, 22341303, 22103079 and 22073092), and the Cooperation Project between Jilin Province and CAS (No. 2023SYHZ0003). Y. Ruan expresses gratitude to Dr. J. Ramírez for assistance with the RepTate software.

REFERENCES

1 Doi, M.; Edwards, S. F. *The theory of polymer dynamics*. Oxford University Press: New York, **1986**.
2 Rubinstein, M.; Colby, R. H. *Polymer Physics*. Oxford University Press: New York, **2003**.
3 Ding, M. M.; Duan, X. Z.; Lu, Y. Y.; Shi, T. F. Statistics of polymer capture by a nanopore: a Brownian dynamics simulation study. *Chinese J. Polym. Sci.* **2015**, *33*, 674–679.
4 Lu, L. W.; Wang, Z. H.; Shi, A. C.; Lu, Y. Y.; An, L. J. Polymer translocation. *Chinese J. Polym. Sci.* **2023**, *41*, 683–698.
5 Mo, J. Y.; Wang, Z. H.; Lu, Y. Y.; An, L. J. Size and dynamics of ring polymers under different topological constraints. *Chinese J. Polym. Sci.* **2023**, *41*, 516–524.
6 Graham, R. S.; Likhtman, A. E.; McLeish, T. C. B.; Milner, S. T. Microscopic theory of linear, entangled polymer chains under rapid deformation including chain stretch and convective constraint release. *J. Rheol.* **2003**, *47*, 1171–1200.
7 Likhtman, A. E.; McLeish, T. C. B. Quantitative theory for linear dynamics of linear entangled polymers. *Macromolecules* **2002**, *35*, 6332–6343.
8 Milner, S. T.; McLeish, T. C. B. Reptation and contour-length fluctuations in melts of linear polymers. *Phys. Rev. Lett.* **1998**, *81*, 725–728.
9 Viovy, J. L.; Rubinstein, M.; Colby, R. H. Constraint release in polymer melts: tube reorganization versus tube dilation. *Macromolecules* **1991**, *24*, 3587–3596.
10 Likhtman, A. E.; Milner, S. T.; McLeish, T. C. B. Microscopic theory for the fast flow of polymer melts. *Phys. Rev. Lett.* **2000**, *85*, 4550–4553.
11 Mead, D. W.; Larson, R. G.; Doi, M. A molecular theory for fast flows of entangled polymers. *Macromolecules* **1998**, *31*, 7895–7914.
12 Costanzo, S.; Huang, Q.; Ianniruberto, G.; Marrucci, G.; Hassager, O.; Vlassopoulos, D. Shear and extensional rheology of polystyrene melts and solutions with the same number of entanglements. *Macromolecules* **2016**, *49*, 3925–3935.
13 Huang, Q.; Hengeller, L.; Alvarez, N. J.; Hassager, O. Bridging the gap between polymer melts and solutions in extensional rheology. *Macromolecules* **2015**, *48*, 4158–4163.
14 Wang, J.; Song, J. H.; Lu, Y. Y.; Ruan, Y. J.; An, L. J. Phase behavior and interfacial properties of diblock copolymer homopolymer ternary mixtures: influence of volume fraction of copolymers and interaction energy. *Chinese J. Polym. Sci.* **2017**, *35*, 874–886.
15 Huang, Q. When polymer chains are highly aligned: a perspective on extensional rheology. *Macromolecules* **2022**, *55*, 715–727.
16 Ianniruberto, G. Extensional flows of solutions of entangled polymers confirm reduction of friction coefficient. *Macromolecules* **2015**, *48*, 6306–6312.
17 Morelly, S. L.; Palmese, L.; Watanabe, H.; Alvarez, N. J. Effect of finite extensibility on nonlinear extensional rheology of polymer melts. *Macromolecules* **2019**, *52*, 915–922.
18 Ianniruberto, G.; Marrucci, G. Molecular dynamics reveals a dramatic drop of the friction coefficient in fast flows of polymer melts. *Macromolecules* **2020**, *53*, 2627–2633.
19 Ianniruberto, G.; Marrucci, G.; Masubuchi, Y. Melts of linear polymers in fast flows. *Macromolecules* **2020**, *53*, 5023–5033.
20 Andreev, M.; Khaliullin, R. N.; Steenbakkers, R. J. A.; Schieber, J. D. Approximations of the discrete slip-link model and their effect on nonlinear rheology predictions. *J. Rheol.* **2013**, *57*, 535–557.
21 Wagner, M. H. Scaling relations for elongational flow of polystyrene melts and concentrated solutions of polystyrene in oligomeric styrene. *Rheol. Acta* **2014**, *53*, 765–777.
22 Shahid, T.; Clasen, C.; Oosterlinck, F.; van Ruymbeke, E. Diluting entangled polymers affects transient hardening but not their steady elongational viscosity. *Macromolecules* **2019**, *52*, 2521–2530.
23 O'Connor, T. C.; Alvarez, N. J.; Robbins, M. O. Relating chain conformations to extensional stress in entangled polymer melts. *Phys. Rev. Lett.* **2018**, *121*, 047801.
24 O'Connor, T. C.; Hopkins, A.; Robbins, M. O. Stress relaxation in highly oriented melts of entangled polymers. *Macromolecules* **2019**, *52*, 8540–8550.
25 Yuan, R.; Liu, J.; Wang, Y.; Wang, S. Q. Uncommon nonlinear

rheological phenomenology in uniaxial extension of polystyrene solutions and melts. *Soft Matter* **2020**, *16*, 3705–3716.
26 Zheng, Y.; Tsige, M.; Wang, S. Q. Molecular dynamics simulation of entangled melts at high rates: identifying entanglement lockup mechanism leading to true strain hardening. *Macromol. Rapid Commun.* **2023**, *44*, 2200159.
27 Baig, C.; Mavrantzas, V. G.; Kröger, M. Flow effects on melt structure and entanglement network of linear polymers: results from a nonequilibrium molecular dynamics simulation study of a polyethylene melt in steady shear. *Macromolecules* **2010**, *43*, 6886–6902.
28 Shanbhag, S.; Kröger, M. Primitive path networks generated by annealing and geometrical methods: insights into differences. *Macromolecules* **2007**, *40*, 2897–2903.
29 Dobson, M. Periodic boundary conditions for long-time nonequilibrium molecular dynamics simulations of incompressible flows. *J. Chem. Phys.* **2014**, *141*, 184103.
30 Murashima, T.; Hagita, K.; Kawakatsu, T. Elongational viscosity of weakly entangled polymer melt *via* coarse-grained molecular dynamics simulation. *Nihon. Reoroji. Gakk.* **2018**, *46*, 207–220.
31 Ruan, Y.; Lu, Y.; An, L.; Wang, Z. G. Multiple entanglements between two chains in polymer melts: an analysis of primitive paths based on Frenet trihedron. *Macromolecules* **2024**, *57*, 2792–2800.
32 Kremer, K.; Grest, G. S. Dynamics of entangled linear polymer melts: a molecular dynamics simulation. *J. Chem. Phys.* **1990**, *92*, 5057–5086.
33 Auhl, R.; Everaers, R.; Grest, G. S.; Kremer, K.; Plimpton, S. J. Equilibration of long chain polymer melts in computer simulations. *J. Chem. Phys.* **2003**, *119*, 12718–12728.
34 Sukumaran, S. K.; Grest, G. S.; Kremer, K.; Everaers, R. Identifying the primitive path mesh in entangled polymer liquids. *J. Polym. Sci., Part B: Polym. Phys.* **2005**, *43*, 917–933.
35 Everaers, R.; Sukumaran, S. K.; Grest, G. S.; Svaneborg, C.; Sivasubramanian, A.; Kremer, K. Rheology and microscopic topology of entangled polymeric liquids. *Science* **2004**, *303*, 823–826.
36 Nosé, S. A molecular-dynamics method for simulations in the canonical ensemble. *Mol. Phys.* **1984**, *52*, 255–268.
37 Hoover, W. G. Canonical dynamics: equilibrium phase-space distributions. *Phys. Rev. A.* **1985**, *31*, 1695–1697.
38 Kröger, M.; Dietz, J. D.; Hoy, R. S.; Luap, C. The Z1+ package: shortest multiple disconnected path for the analysis of entanglements in macromolecular systems. *Comput. Phys. Commun.* **2023**, *283*, 108567.
39 Nicholson, D. A.; Rutledge, G. C. Molecular simulation of flow-enhanced nucleation in n-eicosane melts under steady shear and uniaxial extension. *J. Chem. Phys.* **2016**, *145*, 244903.
40 Todd, B. D.; Daivis, P. J. Homogeneous non-equilibrium molecular dynamics simulations of viscous flow: techniques and applications. *Mol. Simulat.* **2007**, *33*, 189–229.
41 Thompson, A. P.; Aktulga, H. M.; Berger, R.; Bolintineanu, D. S.; Brown, W. M.; Crozier, P. S.; in 't Veld, P. J.; Kohlmeyer, A.; Moore, S. G.; Nguyen, T. D.; Shan, R.; Stevens, M. J.; Tranchida, J.; Trott, C.; Plimpton, S. J. LAMMPS - a flexible simulation tool for particle-based materials modeling at the atomic, meso, and continuum scales. *Comput. Phys. Commun.* **2022**, *271*, 108171.
42 Plimpton, S. Fast parallel algorithms for short-range molecular dynamics. *J. Comput. Phys.* **1995**, *117*, 1–19.
43 Hsu, H. P.; Kremer, K. Static and dynamic properties of large polymer melts in equilibrium. *J. Chem. Phys.* **2016**, *144*, 154907.
44 Ge, T.; Robbins, M. O.; Perahia, D.; Grest, G. S. Healing of polymer interfaces: interfacial dynamics, entanglements, and strength. *Phys. Rev. E.* **2014**, *90*, 012602.
45 Ramírez, J.; Sukumaran, S. K.; Vorselaars, B.; Likhtman, A. E. Efficient on the fly calculation of time correlation functions in computer simulations. *J. Chem. Phys.* **2010**, *133*, 154103.
46 Boudara, V. A. H.; Read, D. J.; Ramírez, J. reptate rheology software: toolkit for the analysis of theories and experiments. *J. Rheol.* **2020**, *64*, 709–722.
47 Huang, Q.; Mednova, O.; Rasmussen, H. K.; Alvarez, N. J.; Skov, A. L.; Almdal, K.; Hassager, O. Concentrated polymer solutions are different from melts: role of entanglement molecular weight. *Macromolecules* **2013**, *46*, 5026–5035.
48 Ma, L. C.; Ruan, Y. J.; Wang, Z. H.; Lu, Y. Y.; An, L. J. Exploring nonlinear rheological behaviors in semi-flexible entangled polymer melts. *Chinese J. Polym. Sci.* **2024**, Doi: 10.1007/s10118-024-3162-0.